IEICE Electronics Express, Vol.17, No.18, 1–6

LETTER

A simple printed antenna with broadband property and omnidirectional radiation patterns of wire dipole

Tuan Hung Nguyen[1, a)], **Ngoc Dong Nguyen**[1], **Hikaru Takizawa**[2], **and Hisashi Morishita**[2]

Abstract This letter presents a unique printed dipole antenna which can roughly cover an 80% fractional bandwidth (VSWR $\leq$ 3), and especially possess the omnidirectional radiation patterns similar to those of wire dipole antenna at its all resonant modes. The antenna is simple with a microstrip-fed structure which it is just composed of two arms with each one forming the shape of a conventional "inset-fed" rectangular patch antenna. At the lowest operation frequency for VSWR = 3, the antenna size is only $0.3\lambda \times 0.008\lambda$, showing its effectiveness in many applications of small antennas.

Keywords: printed dipole antenna, broadband antenna, omnidirectional, wire dipole antenna

Classification: Microwave and millimeter-wave devices, circuits, and modules

1. Introduction

The diversification of smart wireless devices in recent years has been the strongest motivation for the rapid development of various studies on printed antennas [1, 2, 3, 4, 5, 6, 7, 8, 9, 10, 11, 12, 13, 14, 15, 16, 17, 18, 19, 20, 21, 22, 23, 24, 25, 26, 27, 28, 29, 30, 31, 32, 33, 34, 35, 36, 37]. Generally, these antennas can be categorized by the authors into several types such as patches [10, 11, 12], monopoles [13, 14, 15, 16, 17, 18, 19, 20], or dipoles [21, 22, 23, 24, 25, 26, 27, 28, 29, 30, 31, 32, 33, 34, 35, 36, 37]. However, all of them have the most common point in structure, that is, they basically have a planar form which is composed of two conductor parts placed upon two sides of a substrate.

On the other hand, when dealing with these antennas, designers may be possible to obtain dual polarization [4, 5, 35], low cross polarization [13, 26], or a desired radiation pattern [20, 36], but in most works as listed in References, designers often try to increase the antenna's resonant bandwidth by adjusting the shapes of conductor parts on the substrate. Concerning the type of printed dipole antennas [21, 22, 23, 24, 25, 26, 27, 28, 29, 30, 31, 32, 33, 34, 35, 36, 37], although antenna models in these works can provide impressive bandwidth enhancement, other features of some of them may disappear or be unsuitable in some particular applications. For example, the antennas in [22, 24, 26, 27, 31, 32, 33, 34, 36] lose the omnidirectional radiation pattern which is one of the most distinctive feature of an original wire dipole antenna, or those in [21, 25, 29, 32] need an additional balun for balanced feeding. For applications in which omnidirectional radiation pattern in a wide frequency band and the elimination of balun are required, the antenna proposed in this letter can be a good option for designers to choose. Moreover, as described later in the following sessions, the proposed antenna has a unique and interesting property as its three resonant modes are approximately similar to those of a wire dipole antenna with different lengths of $\lambda/4$, $\lambda/2$, and $3\lambda/4$.

[1] Dept. of Radar Technology, Le Quy Don Technical University, 236 Hoang Quoc Viet, Hanoi, Vietnam

[2] Dept. of Electrical and Electronic Engineering, National Defense Academy, 1–10–20 Hashirimizu, Yokosuka, Kanagawa 239–8686, Japan

[a)] hungnt1985_k31@lqdtu.edu.vn

DOI: 10.1587/elex.17.20200261
Received July 28, 2020
Accepted August 4, 2020
Publicized September 14, 2020
Copyedited September 25, 2020

2. Antenna configuration

The configuration of the proposed antenna with different views is shown in Fig. 1. The idea of this configuration is

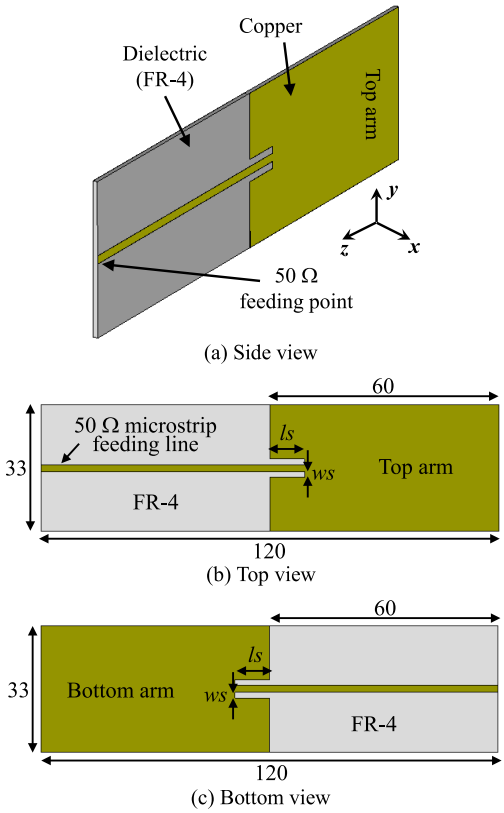

Fig. 1 Different views of the proposed antenna in CST simulation (dimension unit: mm).

inspired from the original microstrip patch antenna [1]. The antenna has two conductor parts (arms) on two opposite sides of a rectangular FR-4 substrate ($\varepsilon_r = 4.8$, $\tan\delta = 0.019$) with the size of $120 \times 33 \times 1$ mm. Both two arms have the identical shape but inverse direction (along z-axis) to each other. This shape is very straightforward and familiar to antenna designers since it is simply the shape of a patch antenna with a microstrip inset-fed structure [1]. For convenience, each arm can be considered to possess a "patch" part and a "line" part whose dimensions are 60×33 mm and 60×1.75 mm, respectively. However, note that due to the microstrip-fed structure, the role of each arm is different to the other. The antenna model in simulation is fed by a waveguide port using the top arm's line part as the feeding line and the bottom arm's patch part as the ground. The width of the line part of the top arm is set to 1.75 mm so that it can provide the characteristic impedance $Z_0 = 50\,\Omega$ matching to the SMA feeding port in practice. The line part of the bottom arm also has a 1.75 mm-width, but in fact, it does not need to be 1.75 mm because it is not a microstrip feeding line. On the other hand, as described later, the slots at the center of the substrate with length ls and width ws of the "inset-fed" parts play an important role in obtaining the broadband characteristic of the antenna.

3. Analysis of antenna characteristics

In this section, we investigate in turn the characteristics of input impedance, radiation pattern, and current distribution of the proposed antenna using the analysis over a frequency band of 500–2000 MHz by Time Domain Solver of the electromagnetic simulator software CST Studio Suite version 2020 [38].

3.1 Input characteristics

First, concerninng the input characteristics of the proposed antenna, to highlight the importance of the slots at the center of the substrate as mentioned above, we focus on the variation of VSWR when changing the slot length ls and the slot width ws. Similar to [3, 8, 15, 18], and our previous works [39, 40, 41], in this letter we also use the criterion of VSWR ≤ 3 ($|S_{11}| \leq -6$ dB) to evaluate the resonant bandwidth of the antenna.

When the slot width ws is fixed to 1.5 mm, and the slot length ls is changed, results of VSWR variation are obtained as indicated in Fig. 2. The antenna's initial shape can be considered as the case with no slots, namely, when $ls = 0$ mm (or $ws = 0$ mm). In this case, VSWR of the antenna is expressed by the thin green solid line in Fig. 2 with the fractional bandwidth for VSWR ≤ 3 is about 39% (844–1254 MHz) with only one resonance at 974 MHz. If ls is increased to 5 mm, two resonances are observed at around 870 MHz and 1100 MHz with better impedance matching as indicated by the thin blue dashed line, and this helps the fractional bandwidth be extended to 52% (800–1362 MHz).

Similarly, the fractional bandwidth continues extending if ls is increased to 9 mm. As expressed by the thick black solid line, when $ls = 9$ mm, not only the 1st and 2nd resonances at 810 MHz and 1190 MHz, but also one more resonance

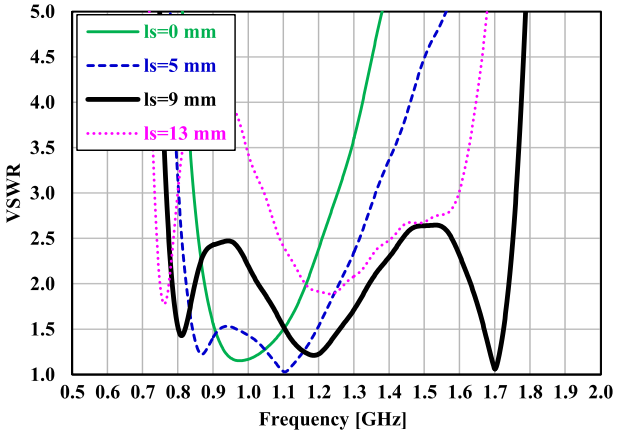

Fig. 2 VSWR characteristics when changing the parameter ls.

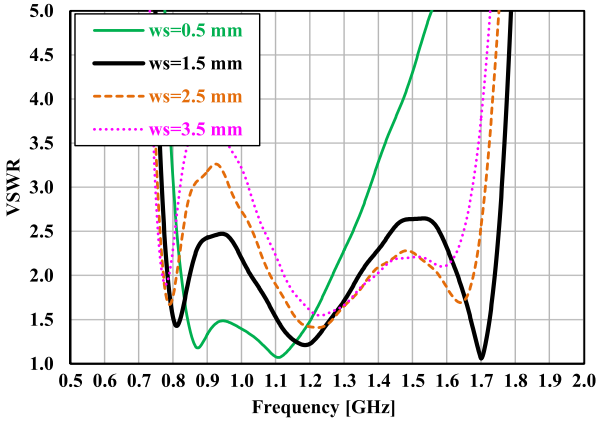

Fig. 3 VSWR characteristics when changing the parameter ws.

appears at 1700 MHz. In this case, the fractional bandwidth is widened to 80% (760–1760 MHz). However, when ls is larger than 9 mm, e.g., $ls = 13$ mm as in the case of the thin pink dotted line, impedance matching between the 1st and 2nd resonances deteriorates, and the bandwidth becomes smaller than the case of $ls = 9$ mm. After conducting a more detailed parameter sweep for ls, we confirmed that when $ws = 1.5$ mm, the value of 9 mm is the best for ls to obtain the widest bandwidth of the antenna.

Next, in the same manner, we investigate the VSWR variation in the case of fixing the slot length ls to 9 mm and changing the slot width ws. It is easy to see in Fig. 3 that with a very narrow slot, e.g., $ws = 0.5$ mm, the 3rd resonance completely vanishes, and the bandwidth degrades with only two resonances remained even though the impedance matching between them becomes better. Comparing Fig. 3 to Fig. 2, we found that the thin green solid line in Fig. 3 ($ws = 0.5$ mm) is relatively similar to the thin blue dashed line ($ls = 5$ mm) in Fig. 2. The cause of this similarity can be assummed that the currents flowing around the slot edges in the both two cases have an approximately indentical effect on input impedance of the antenna.

Also in Fig. 3, when the slot width ws excesses 1.5 mm, e.g., $ws = 2.5$ mm or 3.5 mm, values of VSWR at around 920 MHz increase, and the broadband property of the antenna is not maintained. With a more detailed parameter sweep for ws, we confirmed that when $ls = 9$ mm, in order to attain the widest bandwidth of the antenna, the most

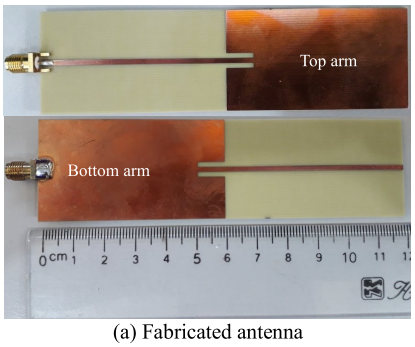

(a) Fabricated antenna

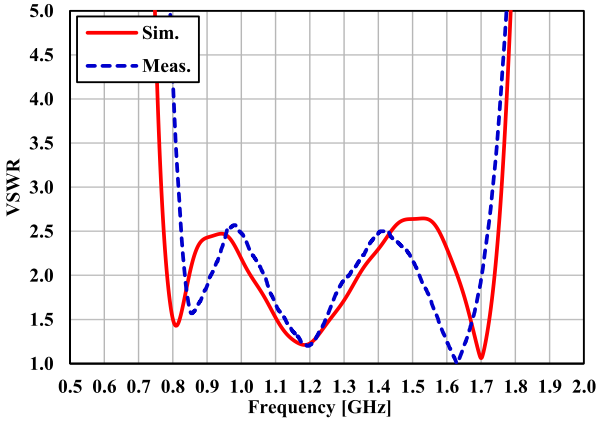

(b) VSWR characteristics

Fig. 4 Fabricated model of the proposed antenna and its measured VSWR characteristic compared to simulation result.

adequate value of ws is 1.5 mm.

From the above results, although no optimization process like in [16, 18, 41] was implemented here, we still can claim that when other dimension parameters of the antenna are fixed as in Fig. 1, the pair of (9 mm, 1.5 mm) is one of the most proper combination of (ls, ws) for achieving the maximally available bandwidth. To validate this claim, we fabricated a practical model of the proposed antenna as shown in Fig. 4(a), and measured its VSWR characteristic compared to simulation results as shown in Fig. 4(b). It is clear in Fig. 4(b) that measurement result is similar to simulated one with three resonant frequencies and the fractional bandwidth of 72% (816–1736 MHz) for VSWR ≤ 3.

To further analyze the importance of the pair (ls = 9 mm, ws = 1.5 mm), in Fig. 5, we address the variation of input impedance in the frequency band around the 3rd resonance (1500–1900 MHz) for the both two cases of changing ls and ws corresponding to Fig. 2 and Fig. 3. In Fig. 5(a), when the slots do not exist (ls = 0 mm) or short (ls = 5 mm), input reactance in 1500-1900 MHz band is completely inductive, but the increment of ls makes the input reactance become more capacitive. However, while ls = 9 mm gives a proper increment of capacitance, ls = 13 mm makes the capacitance increase unnecessarily for matching. Similarly, in Fig. 5(b), the increment of ws also lead to a increment of capacitance, and ws = 1.5 mm provides the most adequate matching condition in this band.

3.2 Radiation patterns and current distributions

In this part, we first investigate the radiation patterns of the prosposed antenna at its three resonant frequencies, namely, f_1 = 0.81 GHz, f_2 = 1.19 GHz, and f_3 = 1.7 GHz. The

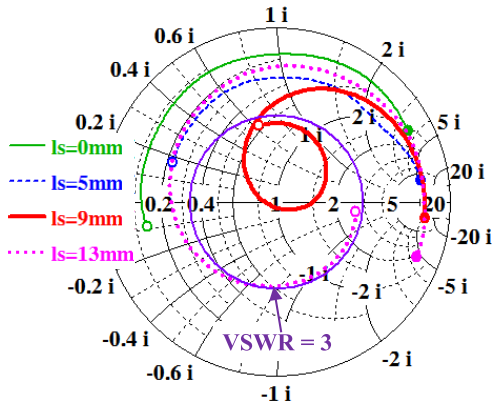

(a) When ws = 1.5 mm and changing ls

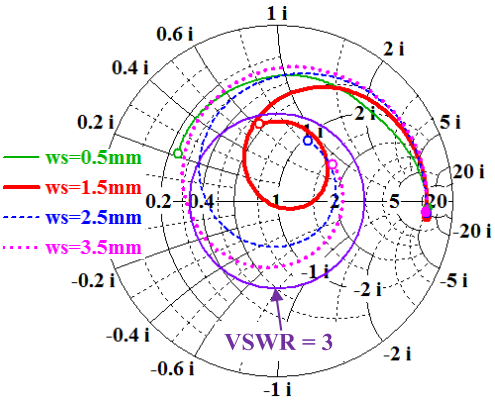

(b) When ls = 9 mm and changing ws

Fig. 5 Variation of normalized input impedance in 1.5–1.9 GHz band.

simulated and measured results of realized gain radiation pattern at these frequencies both in $\boldsymbol{xy}$ and $\boldsymbol{yz}$ planes are respectively shown in Fig. 6(a)–(c). In each plane, since the E_ϕ component is very small, only the E_θ component is plotted. Both simulated and measured results relatively match well to each other. In $\boldsymbol{xy}$ plane, it can be seen that the proposed antenna has omnidirectional radiation patterns at all three frequencies. This is more obvious in $\boldsymbol{yz}$ plane while the proposed antenna has the radiation patterns of "8" shape. These results reveals that radiation patterns of the proposed antenna are close to those of a typical wire dipole antenna [1]. To compare more in details the radiation characteristics between the proposed antenna and a wire dipole antenna, we conduct a detailed analysis as below.

Radiation pattern of an ideal wire dipole antenna which has the length l along z-axis can be expressed by the following function which is excerpted from [1].

$$F(\theta,\phi) = F(\theta) = \left[\frac{\cos\left(\frac{kl}{2}\cos\theta\right) - \cos\left(\frac{kl}{2}\right)}{\sin\theta}\right]^2 \quad (1)$$

where $k = 2\pi/\lambda$ is the wave number. Directivity of the wire dipole antenna is:

$$D_0 = \frac{2F(\theta)|_{\max}}{\int_0^\pi F(\theta)\sin\theta d\theta} \quad (2)$$

Table I summarizes the comparison of radiation quan-

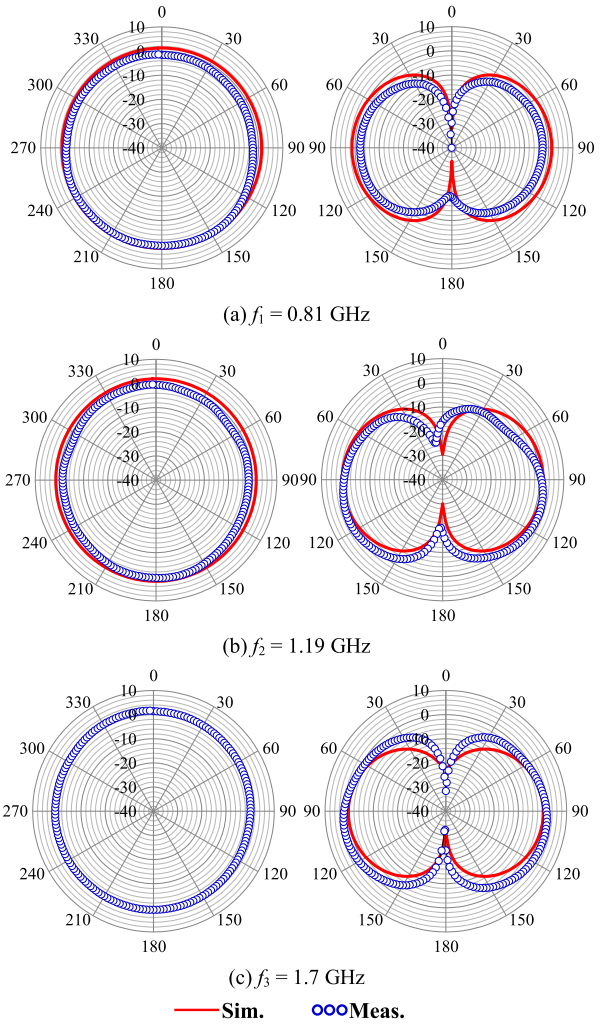

Fig. 6 Simulated and measured realized gain radiation pattern of the proposed antenna at 3 resonant frequencies (unit: dBi; left side: xy-plane; right side: yz-plane).

Table I Comparison between the proposed antenna and wire dipole antenna with different lengths

Half-power beamwidth (*HPBW*)			
Wire dipole antenna	$l = \lambda/4$	$l = \lambda/2$	$l = 3\lambda/4$
	87°	78°	64°
Proposed antenna	f_1	f_2	f_3
	84.4°	77.2°	65.7°
Directivity (D_0 - dimensionless)			
Wire dipole antenna	$l = \lambda/4$	$l = \lambda/2$	$l = 3\lambda/4$
	1.53	1.67	1.92
Proposed antenna	f_1	f_2	f_3
	1.67	1.77	2.15

ties including half-power beamwidth (*HPBW*) and directivity D_0 between the proposed antenna and wire dipole antenna. Quantities of the wire dipole antenna are derived with different values of length l, namely, $l = \lambda/4$, $\lambda/2$, and $3\lambda/4$ [1]. Meanwhile, those of the proposed antenna are extracted from CST simulation result at its three resonant frequencies. It can be seen that the values of both *HBPW* and D_0 of the proposed antenna at f_1 are very close to those of the wire dipole antenna with $l = \lambda/4$. The approximate similarity is also confirmed in the cases of comparing quantities at f_2 and f_3 of the proposed antenna to those of the wire dipole antenna with $l = \lambda/2$ and $l = 3\lambda/4$, respectively.

Next, in Fig. 7, we compare the features of current distributions of the proposed antenna with respect to those of the wire dipole antenna. The normalized value of current amplitude I to a given maximum value I_0 along z-axis of the wire dipole antenna is plotted in Fig. 7(d) based on the formula [1]:

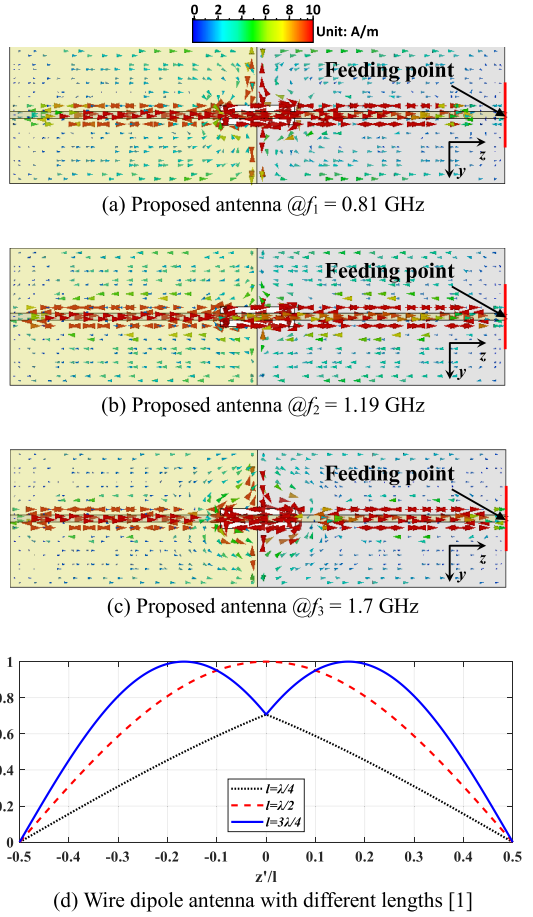

Fig. 7 Comparison of current distributions between the proposed antenna and wire dipole antenna.

$$I = \begin{cases} I_0 \sin\left[k\left(\dfrac{l}{2} - z'\right)\right], & 0 \le z' \le l/2 \\ I_0 \sin\left[k\left(\dfrac{l}{2} + z'\right)\right], & -l/2 \le z' \le 0 \end{cases} \tag{3}$$

in which $z' = 0$ is the center point of the dipole. In Fig. 7(a)–(c), currents that flow on two arms of the proposed antenna are exhibited. We observe that the strongest currents concentrate mainly around the line parts of both two arms of the proposed antenna at all three resonant frequencies. Current distribution at f_1 in Fig. 7(a) is qualitatively similar to the black dotted line ($l = \lambda/4$) in Fig. 7(d). In the same manner, current distributions at f_2 and f_3 in Fig. 7(b), (c) are also relatively similar to the case of $l = \lambda/2$ and $l = 3\lambda/4$ in Fig. 7(d). On the other hand, currents (on the top and bottom arms) that flow along $+y$ and $-y$ directions at the center edges of the substrate are out-of-phase and cancel to each other, and therefore almost have no contribution to the radiation of the proposed antenna.

From the investigation on radiation patterns and current distributions above, we find out that the proposed antenna operates like a $\lambda/4$ wire dipole at its 1st resonance, like a $\lambda/2$

Table II Comparison between the proposed antenna and the others picked up from several references

	Size at f_{min} of VSWR = 3	Fractional bandwidth (VSWR ≤ 3)	Balun need?	Radiation patterns
Antenna in [21]	$0.35\lambda \times 0.03\lambda$	55%	Yes	Omnidirectional at 2 resonances
Antenna in [25]	$0.52\lambda \times 0.1\lambda$	77%	Yes	Nearly omnidirectional at 2 resonances
Antenna in [29]	$0.4\lambda \times 0.2\lambda$	43%	Yes	Omnidirectional at 2 resonance
Antenna in [33]	$0.64\lambda \times 0.12\lambda$	> 100%	No	Directional in all band
Antenna in [37]	$0.38\lambda \times 0.38\lambda$	28% + 21%	No	Omnidirectional at 2 resonances
This work	$0.3\lambda \times 0.08\lambda$	80%	No	Omnidirectional at 3 resonances

wire dipole at its 2nd resonance, and like a $3\lambda/4$ wire dipole at its 3rd resonance. That is to say, the proposed antenna can maintain the features of wire dipole antenna over the entire resonant band. This is a very interesting and distinctive feature of the proposed antenna that differs from the other printed dipoles in [21, 22, 23, 24, 25, 26, 27, 28, 29, 30, 31, 32, 33, 34, 35, 36, 37].

To compare more in details the proposed antenna with the others in [21, 22, 23, 24, 25, 26, 27, 28, 29, 30, 31, 32, 33, 34, 35, 36, 37], we pick up several examples of printed dipole antenna from these references and conduct the comparison. Table II shows the statistical data of the printed dipole antennas in [21, 25, 29, 33, 37] and the proposed antenna in this work. These data include the normalized antenna size with respect to the wavelength λ at the minimum operation frequency of VSWR = 3, the fractional bandwidth for VSWR $\leq$ 3, the requirement of a balun in feeding, and the shapes of radiation patterns at resonant frequencies of each antenna. The data clearly demonstrate the helpful advantages of the proposed antenna as it possesses a small size, the ability of covering a very wide bandwidth and maintaining omnidirectional radiation patterns at its all resonant frequencies without the requirement of a balun in practice.

4. Conclusion

In this letter, a unique printed dipole antenna has been proposed, and its operation features have been analyzed in details. Analysis results revealed that the proposed antenna has a small size, covers roughly 80% fractional bandwidth for VSWR $\leq$ 3 with simple microstrip feeding structure, and moreover, maintains the typical radiation properties of wire dipole antenna with three resonant modes of $\lambda/4$, $\lambda/2$, and $3\lambda/4$. Although its impedance matching over the entire band still needs to be improved further, it can be used in several LTE bands such as Band 5 (824–894 MHz), Band 8 (880–960 MHz), Band 11 (1427.9–1495.9 MHz), or GPS bands such as L1 (1575.42 MHz), L2 (1227.60 MHz). The same antenna structure may also be a proper option for researchers dealing with other frequency bands. In future works, the improvement of impedance matching should be focused, and the utilization of this antenna to construct other antenna structures for particular applications should be considered carefully.

References

[1] C.A. Balanis: *Antenna Theory: Analysis and Design* (John Wiley & Sons, New Jersey, 2016) 4th ed.

[2] S. Soltani and R.D. Murch: "A compact planar printed MIMO antenna design," IEEE Trans. Antennas Propag. **63** (2015) 1140 (DOI: 10.1109/TAP.2015.2389242).

[3] C. Deng, *et al.*: "Planar printed multi-resonant antenna for octa-band WWAN-LTE mobile handset," IEEE Antennas Wireless Propag. Lett. **14** (2015) 1734 (DOI: 10.1109/LAWP.2015.2421335).

[4] W. Li, *et al.*: "Dual-polarized H-shaped printed slot antenna," IEEE Antennas Wireless Propag. Lett. **16** (2016) 1484 (DOI: 10.1109/LAWP.2016.2646805).

[5] W. Li, *et al.*: "Compact dual-polarized printed slot antenna," IEEE Antennas Wireless Propag. Lett. **16** (2017) 2816 (DOI: 10.1109/LAWP.2017.2748542).

[6] Y. Dong, *et al.*: "Folded strip/slot antenna with extended bandwidth for WLAN application," IEEE Antennas Wireless Propag. Lett. **16** (2016) 673 (DOI: 10.1109/LAWP.2016.2598276).

[7] A. Michel, *et al.*: "Printed wideband antenna for LTE-band automotive applications," IEEE Antennas Wireless Propag. Lett. **16** (2016) 1245 (DOI: 10.1109/LAWP.2016.2629619).

[8] Z. Du, *et al.*: "A novel compact wide-band planar antenna for mobile handsets," IEEE Trans. Antennas Propag. **54** (2006) 613 (DOI: 10.1109/TAP.2005.863088).

[9] J.N. Lee and J.K. Park: "Impedance characteristics of trapezoidal ultra-wideband antennas with a notch function," Microw. Opt. Tech. Lett. **46** (2005) 503 (DOI: 10.1002/mop.21029).

[10] Z. Ding, *et al.*: "Broadband antenna design with integrated CB-CPW and parasitic patch structure for WLAN, RFID, Wimax, and 5G applications," IEEE Access **8** (2020) 42877 (DOI: 10.1109/ACCESS.2020.2977616).

[11] W. An, *et al.*: "Low-profile wideband slot-loaded patch antenna with multiresonant modes," IEEE Antennas Wireless Propag. Lett. **17** (2018) 1309 (DOI: 10.1109/LAWP.2018.2843440).

[12] H. Lu, *et al.*: "Capacitive probe-compensation-fed wideband patch antenna with U-shaped parasitic elements for 5G/WLAN/WiMAX applications," IEICE Electron. Express **16** (2019) 20190362 (DOI: 10.1587/elex.16.20190362).

[13] A. Panahi, *et al.*: "A simple polarization reconfigurable printed monopole antenna," IEEE Trans. Antennas Propag. **63** (2015) 5129 (DOI: 10.1109/TAP.2015.2474745).

[14] M.G.N. Alsath and M. Kanagasabai: "Compact UWB monopole antenna for automotive communications," IEEE Trans. Antennas Propag. **63** (2015) 4204 (DOI: 10.1109/TAP.2015.2447006).

[15] Y. Liu, *et al.*: "A planar printed nona-band loop-monopole reconfigurable antenna for mobile handsets," IEEE Antennas Wireless Propag. Lett. **17** (2018) 1575 (DOI: 10.1109/LAWP.2018.2856459).

[16] J. Kim, *et al.*: "Design of an ultra wide-band printed monopole antenna using FDTD and genetic algorithm," IEEE Microw. Wireless Compon. Lett. **15** (2005) 395 (DOI: 10.1109/LMWC.2005.850468).

[17] S.-B. Chen, *et al.*: "Modified T-shaped planar monopole antenna for multiband operation," IEEE Trans. Microw. Theory Techn. **54** (2006) 3267 (DOI: 10.1109/TMTT.2006.877811).

[18] S. Radiom, *et al.*: "Optimised small-size tapered monopole antenna for pulsed ultra-wideband applications designed by a genetic algorithm," IET Microw. Antennas Propag. **3** (2009) 663 (DOI: 10.1049/iet-map.2008.0195).

[19] Y.-L. Kuo and K.-L. Wong: "Printed double-T monopole antenna for 2.4/5.2 GHz dual-band WLAN operations," IEEE Trans. Antennas Propag. **51** (2003) 2187 (DOI: 10.1109/TAP.2003.816391).

[20] S. Liu, *et al.*: "Wideband monopole-like radiation pattern circular patch antenna with high gain and low cross-polarization," IEEE Trans. Antennas Propag. **64** (2016) 2042 (DOI: 10.1109/TAP.2016.2536418).

[21] Y.-W. Chi, *et al.*: "Broadband printed dipole antenna with a step-shaped feed gap for DTV signal reception," IEEE Trans. Antennas Propag. **55** (2007) 3353 (DOI: 10.1109/TAP.2007.908848).

[22] F. Farzami, *et al.*: "Pattern reconfigurable printed dipole antenna using loaded parasitic elements," IEEE Antennas Wireless Propag.

Lett. **16** (2016) 1151 (DOI: 10.1109/LAWP.2016.2625797).
[23] J.-H. Kim, *et al.*: "A printed fan-shaped meandered dipole antenna with mutual-coupled dual resonance," IEEE Antennas Wireless Propag. Lett. **16** (2017) 3168 (DOI: 10.1109/LAWP.2017.2766248).
[24] H. Zong, *et al.*: "Design and analysis of a coupling-fed printed dipole array antenna with high gain and omnidirectivity," IEEE Access **5** (2017) 26501 (DOI: 10.1109/ACCESS.2017.2768518).
[25] A.R. Behera and A.R. Harish: "A novel printed wideband dipole antenna," IEEE Trans. Antennas Propag. **60** (2012) 4418 (DOI: 10.1109/TAP.2012.2207042).
[26] Z. Zhou, *et al.*: "A novel broadband printed dipole antenna with low cross-polarization," IEEE Trans. Antennas Propag. **55** (2007) 3091 (DOI: 10.1109/TAP.2007.908570).
[27] Y. Zhang and H.Y.D. Yang: "Bandwidth-enhanced electrically small printed folded dipoles," IEEE Antennas Wireless Propag. Lett. **9** (2010) 236 (DOI: 10.1109/LAWP.2010.2046875).
[28] S.X. Ta, *et al.*: "Broadband printed-dipole antenna and its arrays for 5G applications," IEEE Antennas Wireless Propag. Lett. **16** (2017) 2183 (DOI: 10.1109/LAWP.2017.2703850).
[29] M. Nagatoshi, *et al.*: "Broadband characteristics of a planar folded dipole antenna with a feed line," IEICE Trans. Commun. **E94-B** (2011) 1168 (DOI: 10.1587/transcom.E94.B.1168).
[30] T. Ma, *et al.*: "Design of novel broadband endfire dipole array antennas," IEEE Antennas Wireless Propag. Lett. **16** (2017) 2935 (DOI: 10.1109/LAWP.2017.2753820).
[31] J.-M. Floc and A.E.S. Ahmad: "Dual-band printed dipole antenna with parasitic element for compensation of frequency space attenuation," Int. J. Electromag. Appl. **2** (2012) 120 (DOI: 10.5923/j.ijea.20120205.05).
[32] C.-H. Ku, *et al.*: "Compact planar dual-band folded dipole antenna for WLAN/WiMAX applications," IEICE Electron. Express **8** (2011) 64 (DOI: 10.1587/elex.8.64).
[33] D.T. Le, *et al.*: "A new scheme to enhance bandwidth of printed dipole for wideband applications," IEICE Trans. Commun. **E97-B** (2014) 773 (DOI: 10.1587/transcom.E97.B.773).
[34] Y. Gou, *et al.*: "A compact dual-polarized printed dipole antenna with high isolation for wideband base station applications," IEEE Trans. Antennas Propag. **62** (2014) 4392 (DOI: 10.1109/TAP.2014.2327653).
[35] P. Knott: "Design of a printed dipole antenna array for a passive radar system," Int. J. Antennas Propag. **2013** (2013) 179296 (DOI: 10.1155/2013/179296).
[36] W. An, *et al.*: "Low-profile and wideband dipole antenna with unidirectional radiation pattern for 5G," IEICE Electron. Express **15** (2018) 20180121 (DOI: 10.1587/elex.15.20180121).
[37] P. Wu, *et al.*: "Multiband antennas comprising multiple frame-printed dipoles," IEEE Trans. Antennas Propag. **57** (2009) 3313 (DOI: 10.1109/TAP.2009.2029371).
[38] Dassault Systems: "CST Studio Suite," ver. 2020, https://www.3ds.com/.
[39] T.H. Nguyen, *et al.*: "A study on minimization of requisite design volume of small antennas inside handset terminals," IEICE Trans. Commun. **E97-B** (2014) 2395 (DOI: 10.1587/transcom.E97.B.2395).
[40] T.H. Nguyen, *et al.*: "Investigation on a multi-band inverted-F antenna sharing only one shorting strip among multiple branch elements," IEICE Trans. Commun. **E98-B** (2015) 1302 (DOI: 10.1587/transcom.E98.B.1302).
[41] T.H. Nguyen, *et al.*: "Space-saving and broadband design of a small vertical U-shaped folded dipole antenna for dual-band WiMAX using a PSO algorithm," IEICE Commun. Express **1** (2012) 89 (DOI: 10.1587/comex.1.89).